Available online at www.sciencedirect.com
SCIENCE DIRECT®
Journal of Computational Physics 201 (2004) 376–395
JOURNAL OF COMPUTATIONAL PHYSICS
www.elsevier.com/locate/jcp

Numerical simulation of a generalized Zakharov system ☆

Shi Jin [a,b,*], Peter A. Markowich [c], Chunxiong Zheng [b]

[a] Department of Mathematics, University of Wisconsin, Madison, WI 53706, USA
[b] Department of Mathematical Science, Tsinghua University, Beijing 100084, PR China
[c] Department of Mathematics, University of Vienna, Nordbergstrasse 15, A-1000 Vienna, Austria

Received 22 March 2004; received in revised form 1 June 2004; accepted 1 June 2004
Available online 15 July 2004

Abstract

In this paper, we propose and study two time-splitting spectral methods for the generalized Zakharov system. These methods are spectrally accurate in space, second order in time, and unconditionally stable. The unconditional stability of the methods offers greater numerical efficiency than those given in previous papers, especially in the subsonic regime. Our numerical experiments confirm the accuracy and stability. In particular, we analyze their behavior in the subsonic regime. The first method, using the exact time integration in phase space for the wave equation for the nondispersive field, converges *uniformly* with respect to the sound speed for the dispersive wave field, while the second method, using the Crank–Nicolson method in the same step, with an initial layer fix by an L-stable time discretization, converges *uniformly* with respect to the sound speed for *both* dispersive and nondispersive fields. Using these new methods we also study the collision behavior of two solitons, in the subsonic region as well as the transsonic region. We obtain numerical results which are quantitatively different from those reported in previous papers using lower resolution numerical techniques.

1. Introduction

This work is aimed at developing efficient numerical schemes for a generalized Zakharov system (ZS) of plasma physics

$$iu_t + u_{xx} + 2\lambda|u|^2u + 2nu = 0,$$

$$\frac{1}{c^2}n_{tt} - n_{xx} + \mu(|u|^2)_{xx} = 0,$$

☆ Research supported in part by US National Science Foundation Grant No. DMS-0305080, National Natural Science Foundation of China Project 10228101, the Basic Research Projects of Tsinghua University under the Project JC2002010, the Wittgenstein Award 2000 financed by the Austria Science Fund and the Austrian–Chinese Scientific–Technological Cooperation Agreement funded by the OEAD (Austria).

* Corresponding author. Tel.: +1-608-263-3302; fax: +1-608-263-8891.
E-mail addresses: jin@math.wisc.edu (S. Jin), czheng@math.tsinghua.edu.cn (C. Zheng).
URL: www.peter-markowich.net. ">"

0021-9991/$ - see front matter © 2004 Elsevier Inc. All rights reserved.
doi:10.1016/j.jcp.2004.06.001

where the complex, dispersive field u is the varying envelope of a highly oscillatory electric field, and the real, nondispersive field n is the fluctuation of the plasma ion density from its equilibrium state. The parameters λ, c and μ are real numbers. This system is a universal model for the study of the interaction between dispersive and nondispersive waves. When $\lambda = 0$, $\mu = 1$, this system is reduced to the classical ZS of plasma physics. When the sound speed $c \to +\infty$, the so-called subsonic limit, the ZS becomes the cubically nonlinear (defocusing if $\lambda + \mu < 0$, focusing if $\lambda + \mu > 0$) Schrödinger equation.

Up to now, many numerical methods have been proposed for the ZS system. For example, Payne et al. [18] designed a spectral method for a 1D ZS. They used a truncated Fourier expansion in their scheme to eliminate the aliasing errors. Glassey [11] presented an energy-preserving finite difference scheme for the ZS in one dimension, and proved its convergence in [12]. In [8,9], Chang et al. presented a conservative difference scheme for the generalized Zakharov system. This scheme can be implicit or semi-explicit depending on the choice of a parameter. They also proved the convergence of their method. More recently, Bao et al. [4] proposed a time-splitting spectral scheme to solve the generalized ZS. Their method was also extended to the vector ZS for multi-component plasmas [3]. Their time-splitting spectral method is a natural extension of a time-splitting method previously used for linear and nonlinear Schrödinger equations (see for example [16]), which was shown to be particularly effective in the semi-classical regime [1,2].

In this paper, we present time-splitting spectral methods different from that in [3,4]. The main difference is that in the splitting step for the nondispersive field equation, we perform the time integration either *exactly* (hereafter called TSSP1), or via the Crank–Nicolson method based on the first order formulation of the second order wave equation (TSSP2). These schemes are second order, and *unconditionally stable*. Most importantly, in the subsonic regime, when c is large, the TSSP1 converges *uniformly* with respect to c for the dispersive wave field, while TSSP2, with an initial layer fix by an L-stable time discretization, converges *uniformly* with respect to c for *both* dispersive *and* nondispersive fields. The previous time-splitting spectral methods, developed in [3,4], require both mesh size and time step to be proportional to $1/c$.

The organization of this paper is as follows. In Section 2, we present our time-splitting spectral methods for the generalized ZS. In Section 3, we perform numerical experiments. We analyze the accuracy of our scheme, both in space and in time. Moreover, we study their performance in the subsonic regime, and demonstrate both analytically and numerically how a scheme can converge uniformly with respect to c. In addition, we use the method to study soliton–soliton collisions in various parameter regimes. Of particular interest is that the obtained critical values for μ/λ, which distinguish region of different post-collision behavior of the solution, are different from those previously reported in the literature [14].

2. A time-splitting spectral method

We restrict ourselves to periodic boundary conditions when presenting the spectral methods. This allows us to use the Fourier spectral method. Of course for other boundary conditions one can always replace the Fourier method by a different spectral approach such as the Chebychev method [6].

Consider the following initial boundary value problem of the ZS:

$$\mathrm{i}u_t + u_{xx} + 2\lambda|u|^2u + 2nu = 0, \quad x \in [-L, L], \ \ t \geqslant 0, \tag{1}$$

$$\frac{1}{c^2}n_{tt} - n_{xx} + \mu(|u|^2)_{xx} = 0, \quad x \in [-L, L], \ \ t \geqslant 0, \tag{2}$$

$$u(-L, t) = u(L, t), \quad u_x(-L, t) = u_x(L, t), \quad t \geqslant 0, \tag{3}$$

$$n(-L, t) = n(L, t), \quad n_x(-L, t) = n_x(L, t), \quad t \geqslant 0, \tag{4}$$

$$u(x, 0) = u_0(x), \quad n(x, 0) = n_0(x), \quad n_t(x, 0) = n_1(x), \quad x \in [-L, L], \tag{5}$$

where

$$\int_{-L}^{L} n_1(x)\,\mathrm{d}x = 0.$$

From Eqs. (1) and (2), it is easy to verify that

$$\frac{\mathrm{d}}{\mathrm{d}t}\int_{-L}^{L} |u(x,t)|^2\,\mathrm{d}x = 0, \quad \frac{\mathrm{d}}{\mathrm{d}t}\int_{-L}^{L} n(x,t)\,\mathrm{d}x = 0. \tag{6}$$

Thus we can induce a new unknown function

$$v(x,t) = -\int_{-L}^{x} n_t(y,t)\,\mathrm{d}y,$$

which is a periodic function on $[-L,L]$ introduced for the purpose of deriving discretizations below. The problem (1)–(5) is then equivalent to the following one:

$$\begin{aligned}
&\mathrm{i}u_t + u_{xx} + 2\lambda|u|^2u + 2nu = 0, \quad x \in [-L,L], \ \ t \geqslant 0,\\
&n_t + v_x = 0, \quad x \in [-L,L], \ \ t \geqslant 0,\\
&\frac{1}{c^2}v_t + (n - \mu|u|^2)_x = 0, \quad x \in [-L,L], \ \ t \geqslant 0,\\
&u(-L,t) = u(L,t), \quad u_x(-L,t) = u_x(L,t), \quad t \geqslant 0,\\
&n(-L,t) = n(L,t), \quad n_x(-L,t) = n_x(L,t), \quad t \geqslant 0,\\
&v(-L,t) = v(L,t), \quad v_x(-L,t) = v_x(L,t), \quad t \geqslant 0,\\
&u(x,0) = u_0(x), \quad n(x,0) = n_0(x), \quad v(x,0) = v_0(x) := -\int_{-L}^{x} n_1(y)\,\mathrm{d}y, \quad x \in [-L,L].
\end{aligned}$$

We denote $x_j = -L + \mathrm{j}h$ with $h = 2L/M$. M, an even number, is the total number of grid points. Besides, we denote $t_m = m\Delta t$ as the time points at which we are going to seek the numerical approximations.

We first illustrate our main idea through a simple (thus first order) splitting. From time t_m to t_{m+1}, we split the continuous problem into two subproblems. First, we solve the free Schrödinger equation

$$\mathrm{i}u_t + u_{xx} = 0 \tag{7}$$

with the initial datum $u(t_m)$ in $[t_m, t_{m+1}]$, to obtain $u^* = u(t_{m+1})$. Then, we solve

$$\mathrm{i}u_t + 2\lambda|u|^2u + 2nu = 0, \tag{8}$$

$$n_t + v_x = 0, \tag{9}$$

$$\frac{1}{c^2}v_t + (n - \mu|u|^2)_x = 0 \tag{10}$$

with the initial data u^*, $n(t_m)$ and $v(t_m)$, again in $[t_m, t_{m+1}]$ to obtain $u(t_{m+1})$, $n(t_{m+1})$ and $v(t_{m+1})$. Note that in (8), $|u(x,t)|^2$ remains invariant in time

$$|u(x,t)|^2 = |u(x,t_m)|^2, \quad t \in [t_m, t_{m+1}].$$

Thus, the problem (8)–(10) is equivalent to

$$\mathrm{i}u_t + 2\lambda|u(x,t_m)|^2u + 2nu = 0, \tag{11}$$

$$n_t + v_x = 0, \tag{12}$$

$$\frac{1}{c^2}v_t + (n - \mu|u(x,t_m)|^2)_x = 0. \tag{13}$$

We denote by u_j, n_j and v_j the approximate values of u, n and v at the grid point $x = x_j$, respectively, and define

$$\mathbf{u}(t) = [u_j(t)]_{j=0}^{M-1}, \quad \mathbf{n}(t) = [n_j(t)]_{j=0}^{M-1}, \quad \mathbf{v}(t) = [v_j(t)]_{j=0}^{M-1}.$$

In our method, the spatial derivative is approximated by the Fourier collocation derivative with a smooth cutoff function $r(x)$, i.e.

$$A_x|_{x=x_j} \approx [\mathscr{D}_x\mathbf{A}]_j, \quad \mathscr{D}_x\mathbf{A} = \mathrm{i}\mathscr{F}^{-1}(\mathbf{k}\mathscr{F}(\mathbf{A})),$$
$$\mathbf{k} = \left[\frac{\pi}{L}\tilde{l}r(\tilde{l}h)\right]_{l=0}^{M-1}, \quad \tilde{l} = \begin{cases} l, & 0 \leqslant l < M/2, \\ l - M, & M/2 \leqslant l < M. \end{cases}$$

Here $\mathscr{F}(\cdot)$ and $\mathscr{F}^{-1}(\cdot)$ are the discrete Fourier and inverse Fourier transforms defined by

$$\mathscr{F}(\mathbf{A}) = \left[\sum_{j=0}^{M-1} A_j \mathrm{e}^{-\frac{2\pi\mathrm{i}jl}{M}}\right]_{l=0}^{M-1}, \quad \mathscr{F}^{-1}(\hat{\mathbf{A}}) = \left[\frac{1}{M}\sum_{l=0}^{M-1}\hat{A}_l \mathrm{e}^{\frac{2\pi\mathrm{i}jl}{M}}\right]_{j=0}^{M-1}.$$

We remark that all vectorial operations are performed component by component and have to be understood as limits when the numerator becomes zero. A cut-off function $r(x)$ is used to *reduce the aliasing error* typically occurring in the long time computation. In the rest of this paper, unless stated otherwise, $r(x)$ is set to be 1, i.e., we approximate the spatial derivative with the standard Fourier collocation derivative (see [6]). Eq. (7) is now approximated by

$$\mathrm{i}\mathbf{u}_t + \mathscr{D}_x^2\mathbf{u} = 0.$$

With initial value $\mathbf{u}(t_m) = \mathbf{u}^m$, this problem can be integrated in time exactly

$$\mathbf{u}^* = \mathscr{F}^{-1}(\mathrm{e}^{-\mathrm{i}\mathbf{k}^2\Delta t}\mathscr{F}(\mathbf{u}^m)).$$

Eqs. (12) and (13) are approximated by

$$\mathbf{n}_t + \mathscr{D}_x\mathbf{v} = 0,$$
$$\frac{1}{c^2}\mathbf{v}_t + \mathscr{D}_x(\mathbf{n} - \mu|\mathbf{u}^*|^2) = 0.$$

Denote $\hat{\mathbf{n}} := \mathscr{F}(\mathbf{n})$ and $\hat{\mathbf{v}} := \mathscr{F}(\mathbf{v})$. Then this system is equivalent to, in the Fourier space,

$$\hat{\mathbf{n}}_t + \mathrm{i}\mathbf{k}\hat{\mathbf{v}} = 0, \tag{14}$$

$$\frac{1}{c^2}\hat{\mathbf{v}}_t + \mathrm{i}\mathbf{k}[\hat{\mathbf{n}} - \mu\mathscr{F}(|\mathbf{u}^*|^2)] = 0. \tag{15}$$

We use two different methods to solve this subproblem. The first one, hereafter which will be referred to as *TSSP1*, is to solve it analytically on $[t_m, t_{m+1}]$, namely,

$$\hat{\mathbf{n}}(t) = [\hat{\mathbf{n}}^m - \mu\mathscr{F}(|\mathbf{u}^*|^2)]\cos c\mathbf{k}(t-t_m) - \frac{\mathrm{i}}{c}\hat{\mathbf{v}}^m \sin c\mathbf{k}(t-t_m) + \mu\mathscr{F}(|\mathbf{u}^*|^2),$$
$$\hat{\mathbf{v}}(t) = -\mathrm{i}c[\hat{\mathbf{n}}^m - \mu\mathscr{F}(|\mathbf{u}^*|^2)]\sin c\mathbf{k}(t-t_m) + \hat{\mathbf{v}}^m \cos c\mathbf{k}(t-t_m).$$

Thus then

$$\hat{\mathbf{n}}^{m+1} = [\hat{\mathbf{n}}^m - \mu\mathscr{F}(|\mathbf{u}^*|^2)]\mathbf{c}_v - \frac{\mathrm{i}}{c}\hat{\mathbf{v}}^m\mathbf{s}_v + \mu\mathscr{F}(|\mathbf{u}^*|^2),$$
$$\hat{\mathbf{v}}^{m+1} = -\mathrm{i}c[\hat{\mathbf{n}}^m - \mu\mathscr{F}(|\mathbf{u}^*|^2)]\mathbf{s}_v + \hat{\mathbf{v}}^m\mathbf{c}_v,$$
$$\mathbf{c}_v = \cos(c\mathbf{k}\Delta t), \quad \mathbf{s}_v = \sin(c\mathbf{k}\Delta t).$$

The second one is to use Crank–Nicolson method (will be referred to as *TSSP2*)

$$\frac{1}{\Delta t}(\hat{\mathbf{n}}^{m+1} - \hat{\mathbf{n}}^m) + \frac{\mathrm{i}\mathbf{k}}{2}(\hat{\mathbf{v}}^{m+1} + \hat{\mathbf{v}}^m) = 0,$$
$$\frac{1}{c^2\Delta t}(\hat{\mathbf{v}}^{m+1} - \hat{\mathbf{v}}^m) + \frac{\mathrm{i}\mathbf{k}}{2}[\hat{\mathbf{n}}^{m+1} + \hat{\mathbf{n}}^m - 2\mu\mathscr{F}(|\mathbf{u}^*|^2)] = 0.$$

The purpose of writing the second order wave equation in n into a first order system is just for the use of the Crank–Nicolson method. Therefore,

$$\hat{\mathbf{n}}^{m+1} = \mathbf{w}_1[\hat{\mathbf{n}}^m - \mu\mathscr{F}(|\mathbf{u}^*|^2)] + \mathbf{w}_2\hat{\mathbf{v}}^m + \mu\mathscr{F}(|\mathbf{u}^*|^2),$$
$$\hat{\mathbf{v}}^{m+1} = \mathbf{w}_2 c^2[\hat{\mathbf{n}}^m - \mu\mathscr{F}(|\mathbf{u}^*|^2)] + \mathbf{w}_1\hat{\mathbf{v}}^m,$$
$$\mathbf{w}_1 = \frac{4 - \mathbf{k}^2c^2\Delta t^2}{4 + \mathbf{k}^2c^2\Delta t^2}, \quad \mathbf{w}_2 = \frac{-4\mathrm{i}\mathbf{k}\Delta t}{4 + \mathbf{k}^2c^2\Delta t^2}.$$

After that, Eq. (11) can be integrated, giving

$$\mathbf{u}^{m+1} = \mathbf{u}^* \mathrm{e}^{2\mathrm{i}\Delta t\lambda|\mathbf{u}^*|^2} \mathrm{e}^{2\mathrm{i}\int_{t_m}^{t_{m+1}} \mathbf{n}(\tau)\,\mathrm{d}\tau}.$$

For TSSP1, one uses

$$\mathbf{u}^{m+1} = \mathbf{u}^* \mathrm{e}^{2\mathrm{i}\lambda\Delta t|\mathbf{u}^*|^2} \mathrm{e}^{2\mathrm{i}\mathscr{F}^{-1}(\hat{\mathbf{T}})},$$

where

$$\hat{\mathbf{T}} = [\hat{\mathbf{n}}^m - \mu\mathscr{F}(|\mathbf{u}^*|^2)]\frac{\mathbf{s}_v}{c\mathbf{k}} + \frac{\mathrm{i}}{c}\hat{\mathbf{v}}^m\frac{\mathbf{c}_v - 1}{c\mathbf{k}} + \mu\mathscr{F}(|\mathbf{u}^*|^2)\Delta t.$$

For TSSP2, one has

$$\mathbf{u}^{m+1} \approx \mathbf{u}^* \mathrm{e}^{2\mathrm{i}\Delta t\lambda|\mathbf{u}^*|^2} \mathrm{e}^{\mathrm{i}\Delta t(\mathbf{n}^m + \mathbf{n}^{m+1})}.$$

Here, the trapezoidal rule is used to approximate the integral.

Clearly, either of these two methods leads to an *unconditionally stable* scheme and conserves the discrete l^2-norm of u. Besides, it is easy to prove that these methods are time reversible. Furthermore, if a constant is added to the initial value of the nondispersive field n, all approximations $\mathbf{n}^m$ are shifted by the same value. This leads to the occurrence of a phase factor in the approximations $\mathbf{u}^m$ of the dispersive field and thus $|\mathbf{u}^m|^2$ is left unchanged. Thus both our methods are time transverse invariant, due to the exact time integrations of both splitting steps of the Schrödinger equation.

In order to have second order accuracy in time, one can use the Strang splitting instead (see [20]). Finally, we present the two schemes

1. TSSP1:

$$\mathbf{c}_v = \cos(c\mathbf{k}\Delta t), \quad \mathbf{s}_v = \sin(c\mathbf{k}\Delta t), \tag{16}$$

$$\mathbf{u}^* = \mathscr{F}^{-1}(\mathrm{e}^{-\mathrm{i}\mathbf{k}^2\Delta t/2}\mathscr{F}(\mathbf{u}^m)), \tag{17}$$

$$\hat{\mathbf{n}}^{m+1} = \left[\hat{\mathbf{n}}^m - \mu\mathscr{F}(|\mathbf{u}^*|^2)\right]\mathbf{c}_v - \frac{\mathrm{i}}{c}\hat{\mathbf{v}}^m\mathbf{s}_v + \mu\mathscr{F}(|\mathbf{u}^*|^2), \tag{18}$$

$$\hat{\mathbf{v}}^{m+1} = -\mathrm{i}c\left[\hat{\mathbf{n}}^m - \mu\mathscr{F}(|\mathbf{u}^*|^2)\right]\mathbf{s}_v + \hat{\mathbf{v}}^m\mathbf{c}_v, \tag{19}$$

$$\hat{\mathbf{T}} = [\hat{\mathbf{n}}^m - \mu\mathscr{F}(|\mathbf{u}^*|^2)]\frac{\mathbf{s}_v}{c\mathbf{k}} + \frac{\mathrm{i}}{c}\hat{\mathbf{v}}^m\frac{\mathbf{c}_v - 1}{c\mathbf{k}} + \mu\mathscr{F}(|\mathbf{u}^*|^2)\Delta t, \tag{20}$$

$$\mathbf{u}^{**} = \mathbf{u}^*\mathrm{e}^{2\mathrm{i}\lambda\Delta t|\mathbf{u}^*|^2}\mathrm{e}^{2\mathrm{i}\mathscr{F}^{-1}(\hat{\mathbf{T}})}, \tag{21}$$

$$\mathbf{u}^{m+1} = \mathscr{F}^{-1}(\mathrm{e}^{-\mathrm{i}\mathbf{k}^2\Delta t/2}\mathscr{F}(\mathbf{u}^{**})), \quad m = 0, 1, 2, \ldots \tag{22}$$

2. TSSP2:

$$\mathbf{w}_1 = \frac{4 - \mathbf{k}^2c^2\Delta t^2}{4 + \mathbf{k}^2c^2\Delta t^2}, \quad \mathbf{w}_2 = \frac{-4\mathrm{i}\mathbf{k}\Delta t}{4 + \mathbf{k}^2c^2\Delta t^2}, \tag{23}$$

$$\mathbf{u}^* = \mathscr{F}^{-1}(\mathrm{e}^{-\mathrm{i}\mathbf{k}^2\Delta t/2}\mathscr{F}(\mathbf{u}^m)), \tag{24}$$

$$\hat{\mathbf{n}}^{m+1} = \mathbf{w}_1[\hat{\mathbf{n}}^m - \mu\mathscr{F}(|\mathbf{u}^*|^2)] + \mathbf{w}_2\hat{\mathbf{v}}^m + \mu\mathscr{F}(|\mathbf{u}^*|^2), \tag{25}$$

$$\hat{\mathbf{v}}^{m+1} = \mathbf{w}_2c^2[\hat{\mathbf{n}}^m - \mu\mathscr{F}(|\mathbf{u}^*|^2)] + \mathbf{w}_1\hat{\mathbf{v}}^m, \tag{26}$$

$$\mathbf{u}^{**} = \mathbf{u}^*\mathrm{e}^{2\mathrm{i}\Delta t\lambda|\mathbf{u}^*|^2}\mathrm{e}^{\mathrm{i}\Delta t(\mathbf{n}^m + \mathbf{n}^{m+1})}, \tag{27}$$

$$\mathbf{u}^{m+1} = \mathscr{F}^{-1}(\mathrm{e}^{-\mathrm{i}\mathbf{k}^2\Delta t/2}\mathscr{F}(\mathbf{u}^{**})), \quad m = 0, 1, 2, \ldots \tag{28}$$

Remark 1. The generalization of these schemes to modified forms of the Zakharov system is straightforward. For example, one can add a damping term in the Schrödinger equation (see [4]) and a dissipative term in the wave equation (see [13])

$$\mathrm{i}u_t + u_{xx} + 2\lambda|u|^2u + 2nu + \mathrm{i}\gamma u = 0, \quad \gamma > 0,$$
$$\frac{1}{c^2}n_{tt} - n_{xx} + \mu(|u|^2)_{xx} = \nu n_{txx}, \quad \nu > 0.$$

Remark 2. One can consider the generalized ZS in higher dimensions ($\mathscr{R}^d$)

$$\mathrm{i}u_t + \Delta u + 2\lambda|u|^2u + 2nu = 0,$$
$$\frac{1}{c^2}n_{tt} - \Delta n + \mu\Delta(|u|^2) = 0.$$

If this problem has a good periodic approximation with period $\prod_{j=1}^{d}[-L_j, L_j]$, and the mean value of $n_t(\cdot, t)$ is zero, we introduce

$$v = (-\Delta)^{1/2}n_t.$$

Thus then

$$n_t = (-\Delta)^{1/2} v,$$
$$v_t + c^2(-\Delta)^{1/2}(n - \mu|u|^2) = 0.$$

Here, the operator $(-\Delta)^{1/2}$ is understood in the Fourier space.

Remark 3. It is worthwhile to explain how to generalize this scheme to the vector ZS for multi-component plasmas in three dimensions. The problem reads (see [21])

$$\mathrm{i}\mathbf{E}_t + a\Delta\mathbf{E} + (1-a)\nabla(\nabla\cdot\mathbf{E}) - \alpha\mathbf{E}\sum_{j=1}^{M} n_j + \lambda|\mathbf{E}|^2\mathbf{E} = 0,$$
$$\frac{1}{c_j^2} n_{j,tt} - \Delta n_j + \mu_j|\mathbf{E}|^2 = 0, \quad j = 1, 2, \ldots, M.$$

Analogously, from time t_m to t_{m+1}, we split this problem into two subproblems. The first one is

$$\mathrm{i}\mathbf{E}_t + a\Delta\mathbf{E} + (1-a)\nabla(\nabla\cdot\mathbf{E}) = 0,$$

and the second

$$\mathrm{i}\mathbf{E}_t - \alpha\mathbf{E}\sum_{j=1}^{M} n_j + \lambda|\mathbf{E}|^2\mathbf{E} = 0,$$
$$\frac{1}{c_j^2} n_{j,tt} - \Delta n_j + \mu_j|\mathbf{E}|^2 = 0, \quad j = 1, 2, \ldots, M.$$

The second subproblem is solved just in the same way as mentioned before. The essential difference lies in how to solve the first subproblem. Again, we approximate the spatial derivative with its corresponding collocation derivative. In Fourier space, we have

$$\mathrm{i}\hat{\mathbf{E}}_t - a\xi^{\mathrm{T}}\xi\hat{\mathbf{E}} - (1-a)\xi\xi^{\mathrm{T}}\hat{\mathbf{E}} = 0$$

with $\xi = (\xi_x, \xi_y, \xi_z)^{\mathrm{T}}$. Thus

$$\hat{\mathbf{E}}(t) = \mathrm{e}^{-\mathrm{i}(t-t_m)(a\xi^{\mathrm{T}}\xi\mathbf{I}+(1-a)\xi\xi^{\mathrm{T}})}\hat{\mathbf{E}}(t_m) = \begin{cases} \hat{\mathbf{E}}(t_m), & |\xi| = 0, \\ \mathrm{e}^{-\mathrm{i}(t-t_m)a|\xi|^2}\left[\mathbf{I} + (\mathrm{e}^{-\mathrm{i}(1-a)(t-t_m)|\xi|^2} - 1)\frac{\xi\xi^{\mathrm{T}}}{|\xi|^2}\right]\hat{\mathbf{E}}(t_m), & \text{otherwise.} \end{cases} \tag{29}$$

Here, $\mathbf{I}$ is the 3×3 identity matrix.

3. Numerical experiments

It is well known that the generalized ZS has the family of one-soliton solutions (see [14])

$$u = [\lambda + \mu(1 - v^2/c^2)^{-1}]^{-1/2} 2\mathrm{i}\eta\,\mathrm{sech}(2\eta(x - vt))\mathrm{e}^{\mathrm{i}\left[\frac{v}{2}x - (\frac{v^2}{4} - 4\eta^2)t + \Phi_0\right]}, \tag{30}$$
$$n = \mu(1 - v^2/c^2)^{-1}|u|^2, \tag{31}$$

if the speed v of the soliton satisfies $\lambda + \mu(1 - v^2/c^2)^{-1} > 0$. In this section, we will use these special solutions to test the performance of our scheme.

3.1. Tests on the accuracy and stability

We first consider the propagation of a single subsonic soliton. As a test of the accuracy of our schemes, we set the parameters to be $\lambda = 0,\ \mu = 1,\ c = 1,\ \eta = 0.5,\ v = 0.5,\ \Phi_0 = 0$. At time $t = 2$, this soliton is plotted in Fig. 1. The initial data are the exact soliton data at $t = 0$. We perform the computation on a large interval $[-128, 128]$, i.e. $L = 128$, thus the periodic boundary conditions do not induce an significant error.

To understand the accuracy of the two methods, two relative errors will be used

$$\epsilon_1 = \frac{\|u - u_{h,k}\|_{l^2}}{\|u\|_{l^2}}, \quad \epsilon_2 = \frac{\|n - n_{h,k}\|_{l^2}}{\|n\|_{l^2}},$$

where $u_{h,k}$ and $n_{h,k}$ are the numerical approximation of u and n. We perform our computation on the time interval $[0, 2]$.

Tables 1 and 2 list the space discretization errors at time $t = 2$ when the time step is chosen sufficiently small that it does not contribute to the significant part of the error. Tables 3 and 4 list the time discretization errors at $t = 2$ when the spatial step size is chosen small enough so it does not affect the error. One can see that both schemes are indeed of spectral accuracy in space and second-order accuracy in time.

The aliasing instability introduces significant numerical errors in long time. Thus, we have to utilize a smooth cut-off function (as function was used for the focusing nonlinear Schrödinger equation in [7] if we want to do long-time simulations). For example, in Fig. 2, we show the numerical solution for $|u|^2$ with $L = 128,\ \lambda = 0,\ \mu = 1,\ c = 1,\ \eta = 0.5,\ v = 0.5,\ \Phi_0 = 0$. We computed with $h = 1/8,\ \Delta t = 0.05$ and $r(x) = \mathrm{e}^{-10(x/L)^{16}}$. Indeed, the result is satisfactory.

3.2. Computations in the subsonic regime

As stated before, when $c \to +\infty$, the generalized ZS reduces to the nonlinear Schrödinger equation

$$\mathrm{i}u_t + u_{xx} + 2(\lambda + \mu)|u|^2 u + 2au = 0 \tag{32}$$

and

$$n(x,t) = \mu|u(x,t)|^2 + a,$$

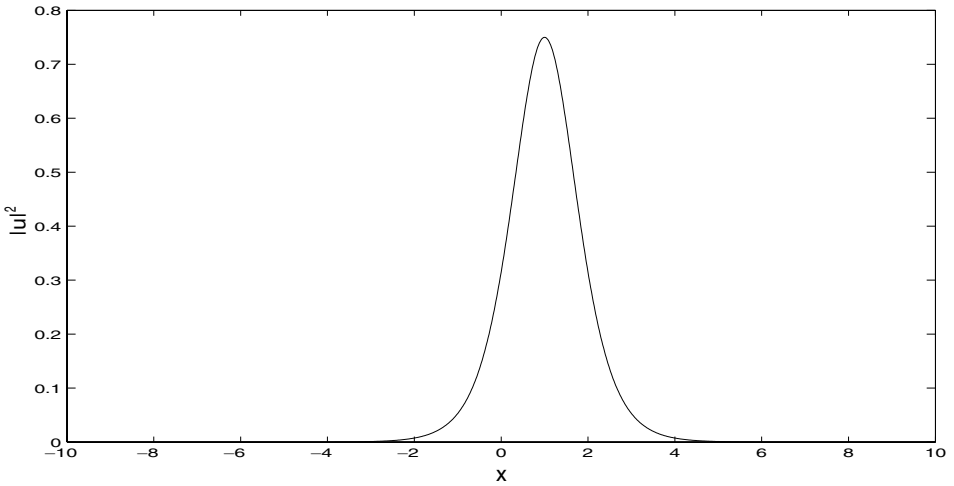

Fig. 1. $|u|^2$-plot of a soliton.

Table 1
TSSP1: ϵ_1 and ϵ_2 at time $t = 2$ with $\Delta t = 1/131072$

Spatial step size	$h = 1$	$h = 1/2$	$h = 1/4$	$h = 1/8$
ϵ_1	0.566E − 1	0.866E − 4	0.115E − 8	0.385E − 10
Order of ϵ_1	–	9.35	16.20	4.90
ϵ_2	0.611E − 1	0.506E − 3	0.951E − 8	0.583E − 10
Order of ϵ_2	–	6.91	15.70	7.35

Table 2
TSSP2: ϵ_1 and ϵ_2 at time $t = 2$ with $\Delta t = 1/131072$

Spatial step size	$h = 1$	$h = 1/2$	$h = 1/4$	$h = 1/8$
ϵ_1	0.425E − 1	0.854E − 4	0.125E − 8	0.417E − 10
Order of ϵ_1	–	8.96	16.06	4.90
ϵ_2	0.656E − 1	0.703E − 3	0.407E − 7	0.500E − 10
Order of ϵ_2	–	6.54	14.08	9.67

Table 3
TSSP1: ϵ_1 and ϵ_2 at time $t = 2$ with $h = 1/32$

Time Step Δt	1/4	1/8	1/16	1/32	1/64	1/128
ϵ_1	0.394E − 1	0.977E − 2	0.245E − 2	0.614E − 3	0.154E − 3	0.384E − 4
Order of ϵ_1	–	2.01	2.00	2.00	2.00	2.00
ϵ_2	0.599E − 1	0.160E − 1	0.408E − 2	0.103E − 2	0.257E − 3	0.642E − 4
Order of ϵ_2	–	1.90	1.97	1.99	2.00	2.00

Table 4
TSSP2: ϵ_1 and ϵ_2 at time $t = 2$ with $h = 1/32$

Time Step Δt	1/4	1/8	1/16	1/32	1/64	1/128
ϵ_1	0.386E − 1	0.962E − 2	0.242E − 2	0.607E − 3	0.152E − 3	0.379E − 4
Order of ϵ_1	–	2.00	1.99	2.00	2.00	2.00
ϵ_2	0.543E − 1	0.140E − 1	0.354E − 2	0.887E − 3	0.222E − 3	0.555E − 4
Order of ϵ_2	–	1.96	1.98	2.00	2.00	2.00

where

$$a = \frac{1}{\mathrm{mes}(\mathscr{B})} \int_{\mathscr{B}} (n(x,t) - \mu|u(x,t)|^2)\,\mathrm{d}x = \frac{1}{\mathrm{mes}(\mathscr{B})} \int_{\mathscr{B}} (n_0(x) - \mu|u_0(x)|^2)\,\mathrm{d}x.$$

Here, $\mathscr{B}$ is the definition domain. The last equality comes from formula (6). Notice that for the problem defined on the whole real axis, we have $a = 0$. This convergence to the nonlinear Schrödinger equation is strong in u, but to obtain a strong convergence $n \to \mu|u|^2 + a$, one needs to impose the compatibility condition

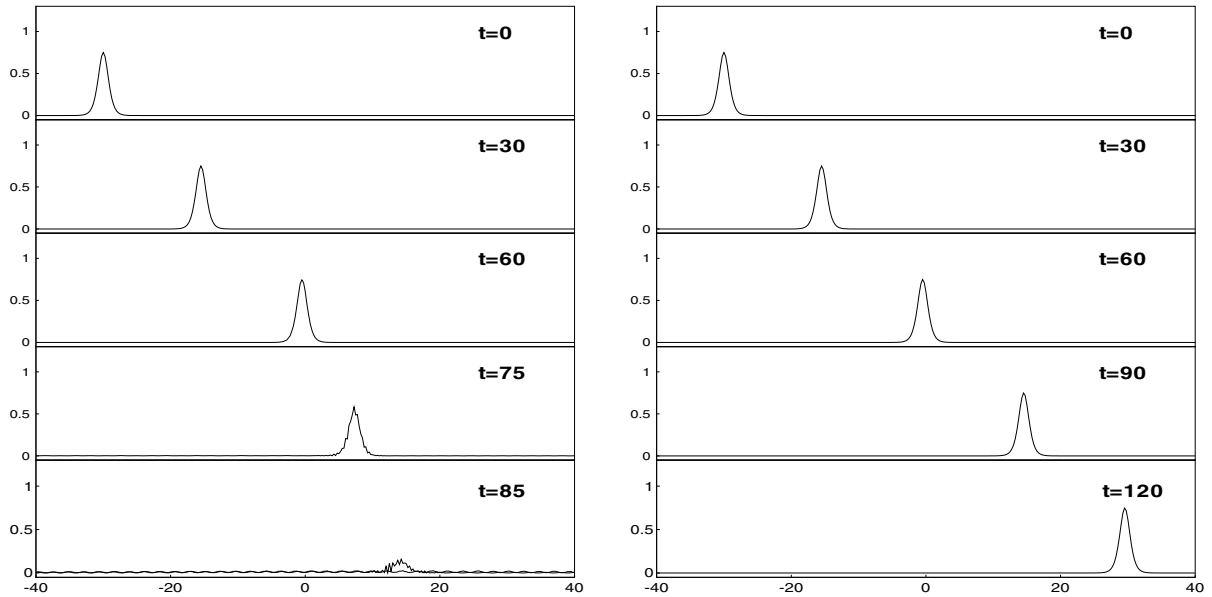

Fig. 2. A soliton moving to the right. Plot of $|u|^2$. $L = 128$, $\eta = 0.5$, $v = 0.5$, $\lambda = 0$, $\mu = 1$. $h = 1/8$, $\Delta t = 1/20$, $r(x) = e^{-10(x/L)^{16}}$. Left: solutions without the exponential cutoff. Right: solutions with the exponential cutoff. TSSP1 is used in the computation.

$$n_0(x) - \mu|u_0(x)|^2 - a = O(1/c) \tag{33}$$

for the initial data [19]. If this compatibility condition is not met by the initial data, there is an oscillatory term that needs to be subtracted in order to establish the strong convergence in n, otherwise only weak convergence in time can be obtained for n [17,21]. This subtle analytical issues concerned with the non-dispersive field n raise some interesting numerical questions which were not addressed in [3,4] but will be studied here.

In this subsection we shall study the performance of the two methods in the regime $c \gg 1$. In particular, we are interested in the relative ratio between mesh size/time step over c^{-1} that can give accurate approximation. As an example, we choose $\lambda = 0$, $\mu = 1$, $L = 128$, and the initial data to be one of the following two sets:

1. Data set one:

$$u_0(x) = i\,\mathrm{sech}(x)e^{\frac{i}{4}x}, \quad n_0(x) = \mathrm{sech}^2(x), \quad n_1(x) = \mathrm{sech}^2(x)\tanh(x).$$

2. Data set two:

$$u_0(x) = i\,\mathrm{sech}(x)e^{\frac{i}{4}x}, \quad n_0(x) = 0, \quad n_1(x) = 0.$$

Clearly the first set meets the compatibility condition, while the second does not.

Consider the data set one first. In this case, $a = 0$, and the exact solution of the Schrödinger equation is

$$u^{\mathrm{NLS}}(x,t) = i\,\mathrm{sech}(x - t/2)e^{i(\frac{1}{4}x + \frac{15}{16}t)}, \quad n^{\mathrm{NLS}}(x,t) = \mathrm{sech}^2(x - t/2). \tag{34}$$

First, we use this example to test the convergence rate of generalized ZS to the nonlinear Schrödinger equation. We compute the numerical solution of ZS with mesh size $h = 1/8$ (which turns out to be small enough since $h = 1/16$ presents almost the same results when other parameters are fixed) and sufficiently small (relative to $1/c$) time step $\Delta t = 0.0005$. Three relative errors will be used

$$\epsilon_3 = \frac{\|u^{\mathrm{GZS}}(t) - u^{\mathrm{NLS}}(t)\|_{l^2}}{\|u^{\mathrm{NLS}}(t)\|_{l^2}}, \quad \epsilon_4 = \frac{\|n^{\mathrm{GZS}}(t) - |u^{\mathrm{NLS}}(t)|^2\|_{l^2}}{\||u^{\mathrm{NLS}}(t)|^2\|_{l^2}}, \quad \epsilon_5 = \frac{\||u^{\mathrm{GZS}}(t)|^2 - |u^{\mathrm{NLS}}(t)|^2\|_{l^1}}{\||u^{\mathrm{NLS}}(t)|^2\|_{l^1}}.$$

Tables 5 and 6 list the results. One can see that the generalized ZS reduces to the nonlinear Schrödinger equation with order $O(1/c^2)$ strongly for u and n.

Tables 7 and 8 list the relative errors when $\Delta t = 1/c$. We see that the numerical solutions of the generalized ZS still converge to the exact solution of the nonlinear Schrödinger equation with order $O(1/c^2)$.

The next set of tests will be to choose the time step independent of the sound speed c. Fig. 3 plots the numerical errors for $\Delta t = 0.01$. One can see that, for fixed h and Δt, as $c \to \infty$, TSSP2 gives good convergence for both u and n to the desired subsonic limit, but TSSP1 fails to give convergence of n to $\mu|u|^2$.

The failure in convergence for n using TSSP1 can be understood as follows. When $c\Delta t \gg 1$, both $\mathbf{c}_v$ and $\mathbf{s}_v$ in (16) are oscillatory functions, and hence $\hat{\mathbf{n}}^{m+1}$ in (18) is oscillatory. Calculating $\mathbf{n}^{m+1}$ requires a discrete Fourier transform of the oscillatory function $\hat{\mathbf{n}}^{m+1}$ which cannot be accurate unless sufficiently small mesh size is used or $c\Delta t = O(1)$. As for the convergence of u, note that in (20), $\hat{T} \to \mu\mathscr{F}(|\mathbf{u}^*|^2)\Delta t$ strongly as $c \to \infty$. Applying this limit in (21), one sees that $\mathbf{u}^*$ in (17) and $\mathbf{u}^{**}$ form exactly the time-splitting spectral method for the nonlinear Schrödinger equation (32) (see [2]).

For TSSP2, no oscillatory terms exist in (25), although a different problem will occur when the initial data does not satisfy the compatibility condition (33), as we will see next.

We now consider the initial data set two, which does not satisfy the compatibility condition (33). In this case, the subsonic limit solution is

$$u^{\mathrm{NLS}}(x,t) = \mathrm{i}\,\mathrm{sech}(x - t/2)\mathrm{e}^{\mathrm{i}(\frac{1}{4}x + \frac{15}{16}t)}\mathrm{e}^{-\frac{2\mathrm{i}t}{L^2}}, \quad n^{\mathrm{NLS}}(x,t) = \mathrm{sech}^2(x - t/2) - \frac{1}{L}.$$

Table 5
Relative errors between the generalized ZS and the corresponding nonlinear Schrödinger equation

	$c = 10$	$c = 20$	$c = 40$	$c = 80$	$c = 160$
ϵ_3	0.205E − 1	0.516E − 2	0.130E − 2	0.323E − 3	0.801E − 4
Order of ϵ_3	–	1.99	1.99	2.01	2.01
ϵ_4	0.451E − 2	0.112E − 2	0.281E − 3	0.701E − 4	0.187E − 4
Order of ϵ_4	–	2.01	1.99	2.00	1.91
ϵ_5	0.235E − 2	0.576E − 3	0.144E − 3	0.359E − 4	0.888E − 5
Order of ϵ_5	–	2.03	2.00	2.00	2.01

The errors are computed at time $t = 4$ with $h = 1/8$ and $\Delta t = 0.0005$. TSSP1 is used.

Table 6
Relative errors between the generalized ZS and the corresponding nonlinear Schrödinger equation

	$c = 10$	$c = 20$	$c = 40$	$c = 80$	$c = 160$
ϵ_3	0.204E − 1	0.513E − 2	0.129E − 2	0.323E − 3	0.794E − 4
Order of ϵ_3	–	1.99	1.99	1.99	2.03
ϵ_4	0.447E − 2	0.112E − 2	0.282E − 3	0.708E − 4	0.182E − 4
Order of ϵ_4	–	1.99	1.99	1.99	1.96
ϵ_5	0.234E − 2	0.575E − 3	0.145E − 3	0.363E − 4	0.891E − 5
Order of ϵ_5	–	2.03	1.99	1.99	2.03

The errors are computed at time $t = 4$ with $h = 1/8$ and $\Delta t = 0.0005$. TSSP2 is used.

Table 7
Relative errors of the numerical solutions of the generalized ZS by TSSP1

	$c = 160$	$c = 320$	$c = 640$	$c = 1280$	$c = 2560$
ϵ_3	0.477E − 4	0.121E − 4	0.303E − 5	0.756E − 6	0.189E − 6
Order of ϵ_3	–	1.98	2.00	2.00	2.00
ϵ_4	0.785E − 3	0.997E − 5	0.248E − 5	0.619E − 6	0.155E − 6
Order of ϵ_4	–	2.98	2.01	2.00	2.00
ϵ_5	0.162E − 4	0.406E − 5	0.102E − 5	0.254E − 6	0.637E − 7
Order of ϵ_5	–	2.00	1.99	2.01	2.00

The errors are computed at time $t = 4$ under $h = 1/8$ and $\Delta t = 1/c$.

Table 8
relative errors of the numerical solutions of the generalized ZS by TSSP2

	$c = 160$	$c = 320$	$c = 640$	$c = 1280$	$c = 2560$
ϵ_3	0.369E − 4	0.921E − 5	0.230E − 5	0.576E − 6	0.144E − 6
Order of ϵ_3	–	2.00	2.00	2.00	2.00
ϵ_4	0.309E − 4	0.758E − 5	0.181E − 5	0.475E − 6	0.115E − 6
Order of ϵ_4	–	2.03	2.07	1.93	2.05
ϵ_5	0.782E − 5	0.195E − 5	0.489E − 6	0.122E − 6	0.305E − 7
Order of ϵ_5	–	2.00	2.00	2.00	2.00

The errors are computed at time $t = 4$ under $h = 1/8$ and $\Delta t = 1/c$.

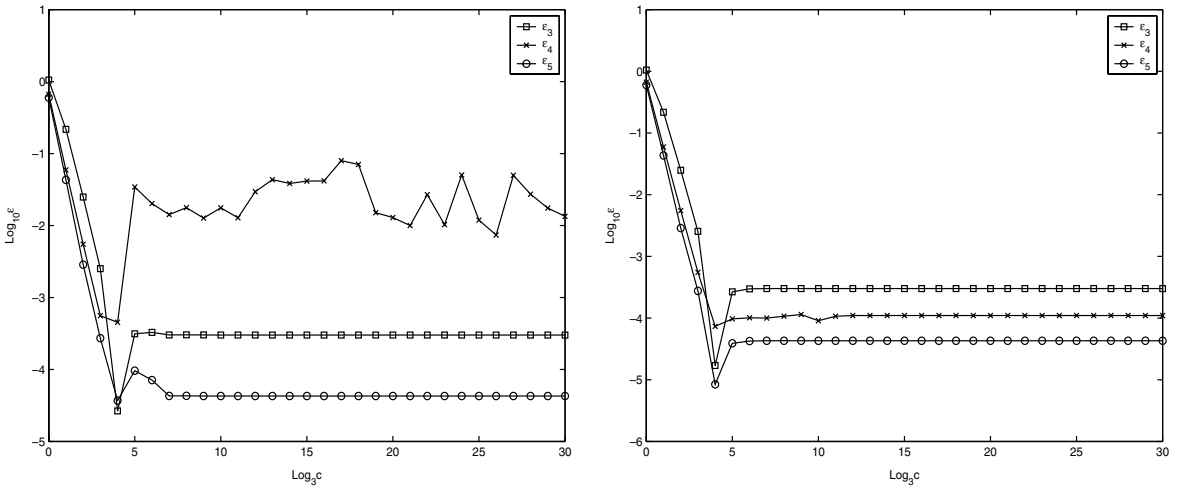

Fig. 3. Plots of the relative errors as $c \to \infty$. The errors are computed at time $t = 4$ under $h = 1/8$. Left: TSSP1. Right: TSSP2.

Fig. 4 plots the numerical solutions. The left subplot shows the numerical solution of n with a very small time step $\Delta t = 0.0001$ using TSSP1. This solution can be taken as the "*exact*" solution. The right one shows the numerical solution of n when TSSP2 is used. The numerical solution n does not converge when $c \to \infty$ while holding Δt fixed.

The reason why this happens can be explained as the following. When $c \to \infty$, in view of Eq. (23), one has

$$\mathbf{w}_1 = \begin{cases} 1, & \mathbf{k} = 0, \\ -1, & \text{otherwise}, \end{cases} \qquad \mathbf{w}_2 = 0.$$

Thus from (25),

$$\hat{\mathbf{n}}^{m+1} + \hat{\mathbf{n}}^m = \begin{cases} 2\hat{\mathbf{n}}^0, & \mathbf{k} = 0, \\ 2\mu\mathscr{F}(|\mathbf{u}^*|^2), & \text{otherwise}. \end{cases}$$

That is to say

$$\mathbf{n}^{m+1} + \mathbf{n}^m = 2\mu|\mathbf{u}^*|^2 + 2a. \tag{35}$$

If we apply this to (27) in TTSP2 one can see $\mathbf{u}^*$ and $\mathbf{u}^{**}$ again form exactly the time-splitting spectral method for the nonlinear Schrödinger equation (33) (see [2]). So u will always converge numerically as $c \to \infty$. However, if $\mathbf{n}^m - \mu|\mathbf{u}^m|^2 - a = \mathrm{O}(1)$ then (35) implies (note that $\mathbf{u}^m - \mathbf{u}^* = \mathrm{O}(\Delta t)$, $\mathbf{u}^{m+1} - \mathbf{u}^* = \mathrm{O}(\Delta t)$),

$$\mathbf{n}^{m+1} - \mu|\mathbf{u}^{m+1}|^2 - a = \mathrm{O}(1).$$

Thus, if the the initial data does not satisfy the compatibility condition (33), such an incompatibility will be preserved at all later time, preventing n from converging to $\mu|u|^2 + a$.

Since this error is mainly caused by the initial incompatibility, one can use L-stable ODE solvers [10] to remove this error. Such phenomenon (initial layer discrepancy) has been studied for hyperbolic systems with stiff relaxation terms, see [5,15], where L-stable ODE solvers were used to eliminate the error introduced by under-resolution of the initial layer. For the ZS problem, one could either replace the Crank–Nicolson (which is not L-stable) method by a second order L-stable ODE solver, or more simply, use an L-stable scheme (such as the backward Euler method) for the first time step. Here we take the second approach. Since we only use the first-order scheme for one time step, the overall accuracy in time remains second order. Below for completeness we list the full scheme (called TSSP2-1)

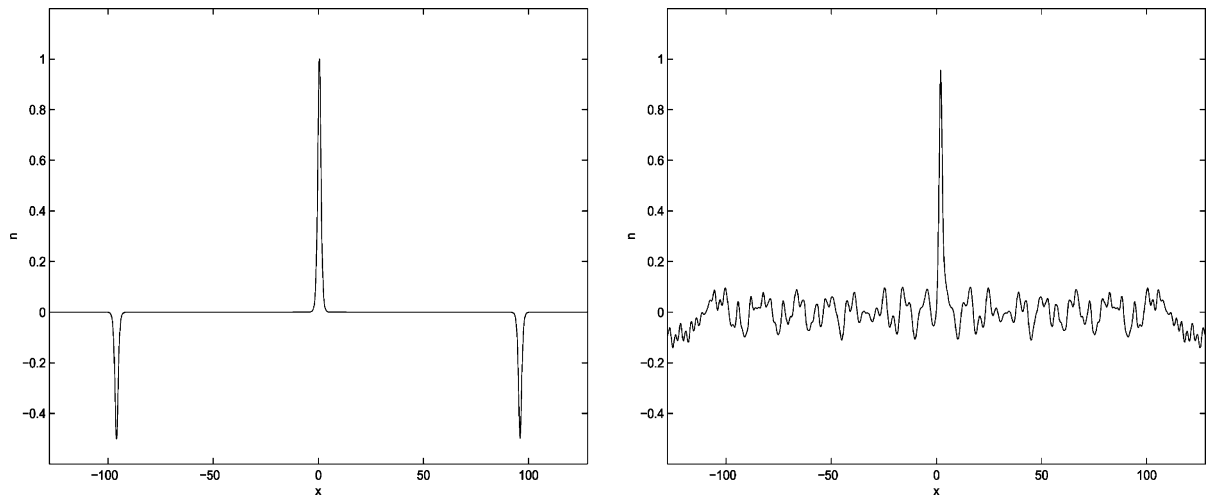

Fig. 4. n-plots: numerical solutions at time $t = 1$ with $h = 1/8$ for $c = 160$. Left: Scheme one with $\Delta t = 0.0001$. Right: Scheme two with $\Delta t = 0.01$.

$$
\begin{aligned}
&\mathbf{w}_1^* = \frac{1}{1+\mathbf{k}^2c^2\Delta t^2}, \quad \mathbf{w}_2^* = \frac{-\mathrm{i}\mathbf{k}\Delta t}{1+\mathbf{k}^2c^2\Delta t^2},\\
&\mathbf{u}^* = \mathscr{F}^{-1}(\mathrm{e}^{-\mathrm{i}\mathbf{k}^2\Delta t}\mathscr{F}(\mathbf{u}^0)),\\
&\hat{\mathbf{n}}^1 = \mathbf{w}_1^*[\hat{\mathbf{n}}^0 - \mu\mathscr{F}(|\mathbf{u}^*|^2)] + \mathbf{w}_2^*\hat{\mathbf{v}}^0 + \mu\mathscr{F}(|\mathbf{u}^*|^2),\\
&\hat{\mathbf{v}}^1 = \mathbf{w}_2^*c^2[\hat{\mathbf{n}}^0 - \mu\mathscr{F}(|\mathbf{u}^*|^2)] + \mathbf{w}_1^*\hat{\mathbf{v}}^0,\\
&\mathbf{u}^1 = \mathbf{u}^*\mathrm{e}^{2\mathrm{i}\Delta t\lambda|\mathbf{u}^*|^2}\mathrm{e}^{2\mathrm{i}\Delta t\mathbf{n}^1},\\
&\mathbf{w}_1 = \frac{4-\mathbf{k}^2c^2\Delta t^2}{4+\mathbf{k}^2c^2\Delta t^2}, \quad \mathbf{w}_2 = \frac{-4\mathrm{i}\mathbf{k}\Delta t}{4+\mathbf{k}^2c^2\Delta t^2},\\
&\mathbf{u}^* = \mathscr{F}^{-1}(\mathrm{e}^{-\mathrm{i}\mathbf{k}^2\Delta t/2}\mathscr{F}(\mathbf{u}^m)),\\
&\hat{\mathbf{n}}^{m+1} = \mathbf{w}_1[\hat{\mathbf{n}}^m - \mu\mathscr{F}(|\mathbf{u}^*|^2)] + \mathbf{w}_2\hat{\mathbf{v}}^m + \mu\mathscr{F}(|\mathbf{u}^*|^2),\\
&\hat{\mathbf{v}}^{m+1} = \mathbf{w}_2c^2[\hat{\mathbf{n}}^m - \mu\mathscr{F}(|\mathbf{u}^*|^2)] + \mathbf{w}_1\hat{\mathbf{v}}^m,\\
&\mathbf{u}^{**} = \mathbf{u}^*\mathrm{e}^{2\mathrm{i}\Delta t\lambda|\mathbf{u}^*|^2}\mathrm{e}^{\mathrm{i}\Delta t(\mathbf{n}^m+\mathbf{n}^{m+1})},\\
&\mathbf{u}^{m+1} = \mathscr{F}^{-1}(\mathrm{e}^{-\mathrm{i}\mathbf{k}^2\Delta t/2}\mathscr{F}(\mathbf{u}^{**})), \quad m = 1,2,\ldots
\end{aligned}
$$

Table 9
Relative errors between numerical solution and *exact* solution for $c = 1E^{10}$ at time $t = 4$ when TSSP2-1 is used

	$\Delta t = 0.02$	$\Delta t = 0.01$	$\Delta t = 0.005$	$\Delta t = 0.0025$
ϵ_3	0.122E − 2	0.304E − 3	0.757E − 4	0.189E − 4
Order of ϵ_3	–	2.00	2.01	2.00
ϵ_4	0.454E − 3	0.114E − 3	0.285E − 4	0.711E − 5
Order of ϵ_4	–	1.99	2.00	2.00

We take the solution of nonlinear Schrödinger equation as the exact solution. The numerical solution is computed with initial data set two.

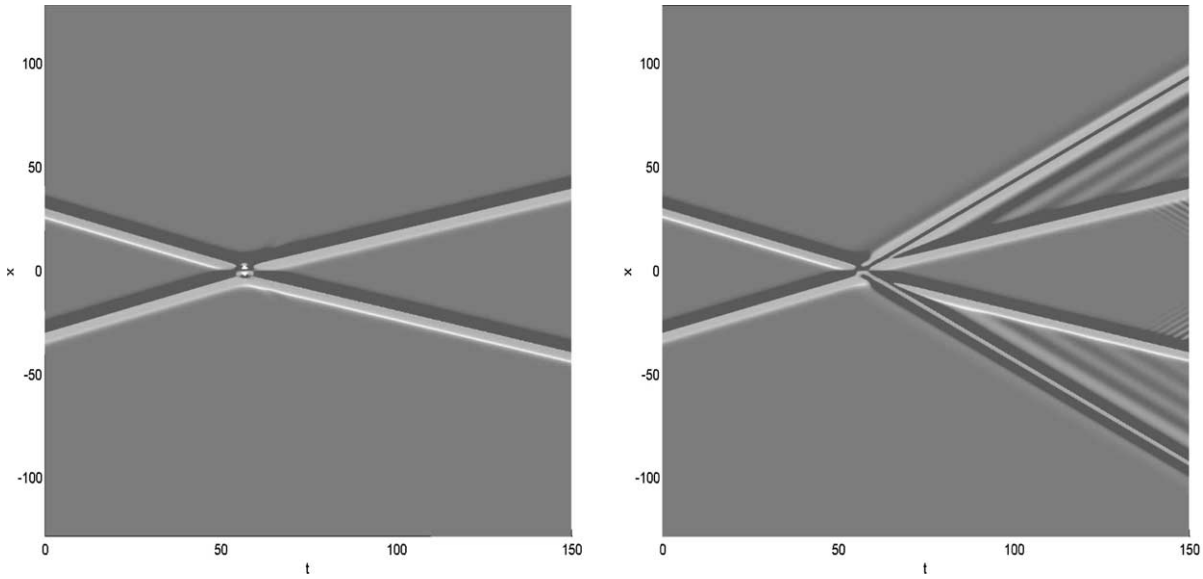

Fig. 5. $v = 0.5$, $\mu/\lambda = 0.02$. Left: $|u|^2$. Right: n.

When $c\Delta t \gg 1$, the backward Euler step clearly drives n to $\mu|u|^2 + a$ after the first time step. This prepares the compatible data right into the subsonic limit, and for all later time the solution will remain in the subsonic limit for n, as can be seen from the above analysis.

Table 9 lists the L^2 relative errors with TSSP2-1. The results agree with our analysis.

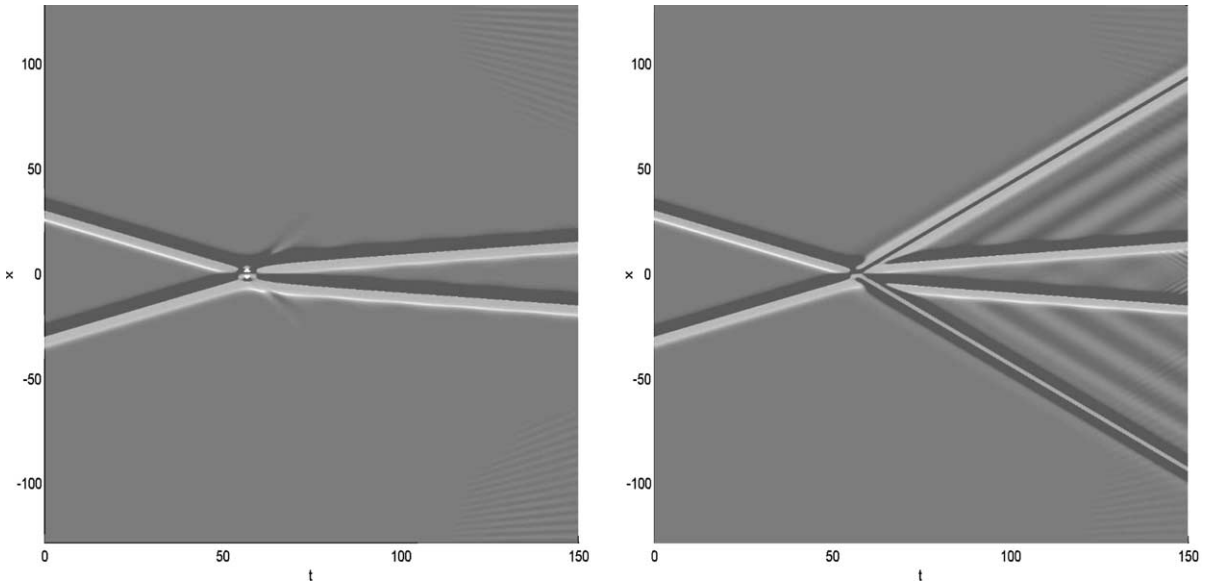

Fig. 6. $v = 0.5$, $\mu/\lambda = 0.06$. Left: $|u|^2$. Right: n.

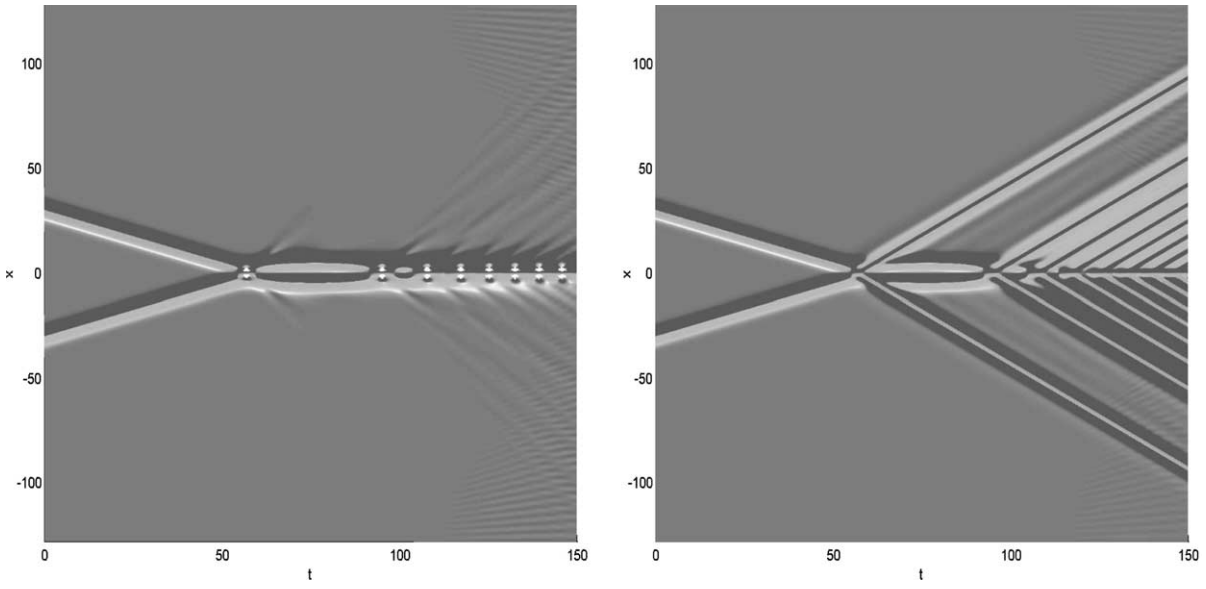

Fig. 7. $v = 0.5$, $\mu/\lambda = 0.07$. Left: $|u|^2$. Right: n.

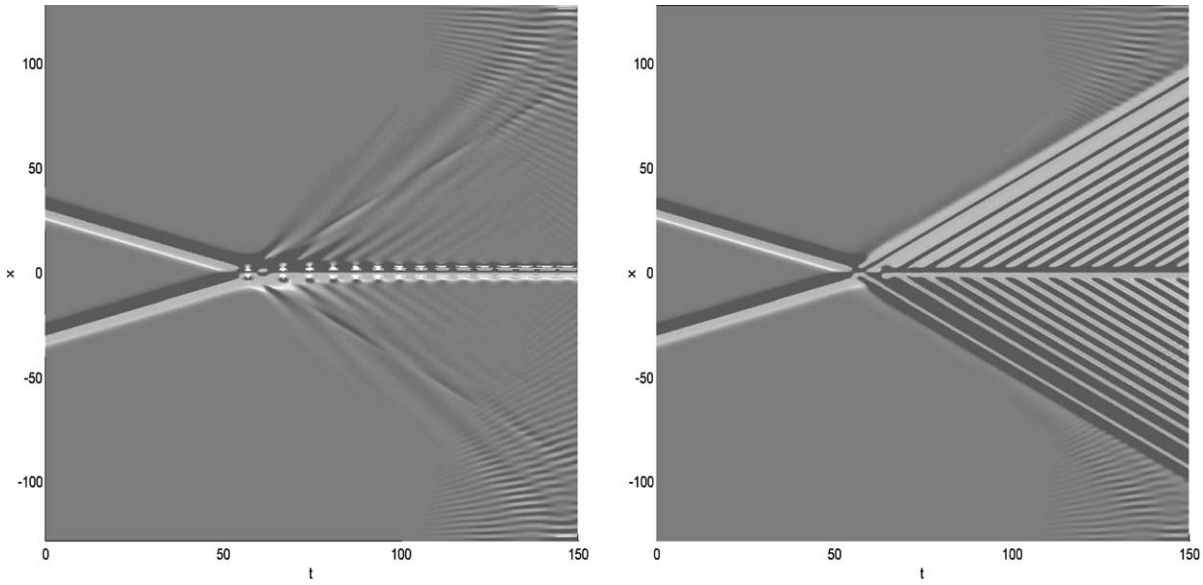

Fig. 8. $v = 0.5$, $\mu/\lambda = 0.2$. Left: $|u|^2$. Right: n.

Table 10
The critical point for different velocity

v	0.1	0.3	0.5	0.7	0.9
μ/λ	$0.0027_{\pm 1}$	$0.025_{\pm 1}$	$0.065_{\pm 1}$	$0.121_{\pm 1}$	>1.0E + 10

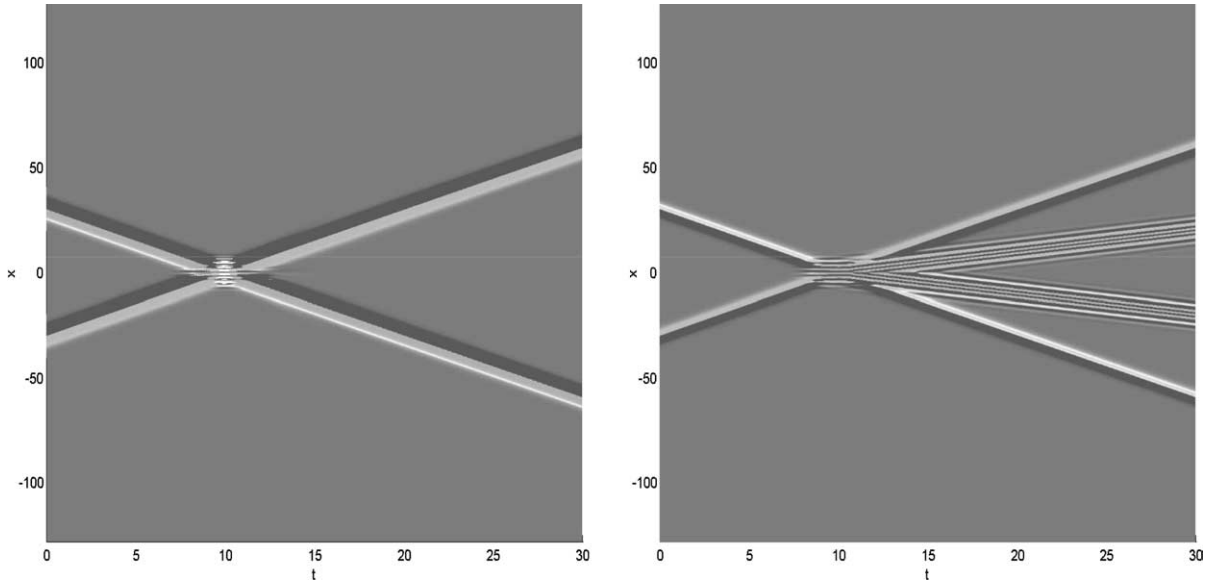

Fig. 9. $v = 3.0$, $\mu/\lambda = 0.2$. Left: $|u|^2$. Right: n.

3.3. Applications to soliton–soliton collisions

In this subsection we use TSSP2 to study the collision of two solitons. For simplicity, we confine ourselves to symmetric collisions with both zero initial phases, i.e. the two solitons have the same speed and same amplitude but propagate in the opposite directions. We set $\eta = 0.3$ and $c = 1$ in the following. All computations are performed with a sufficiently refined mesh $h = 1/32$ and sufficiently small time step $\Delta t = 0.001$.

- $\lambda > 0$ and $\mu > 0$. The solitons exist in two different regimes: subsonic regime

$$|v| < c$$

and transsonic regime

$$|v| > c\sqrt{1 + \mu/\lambda}.$$

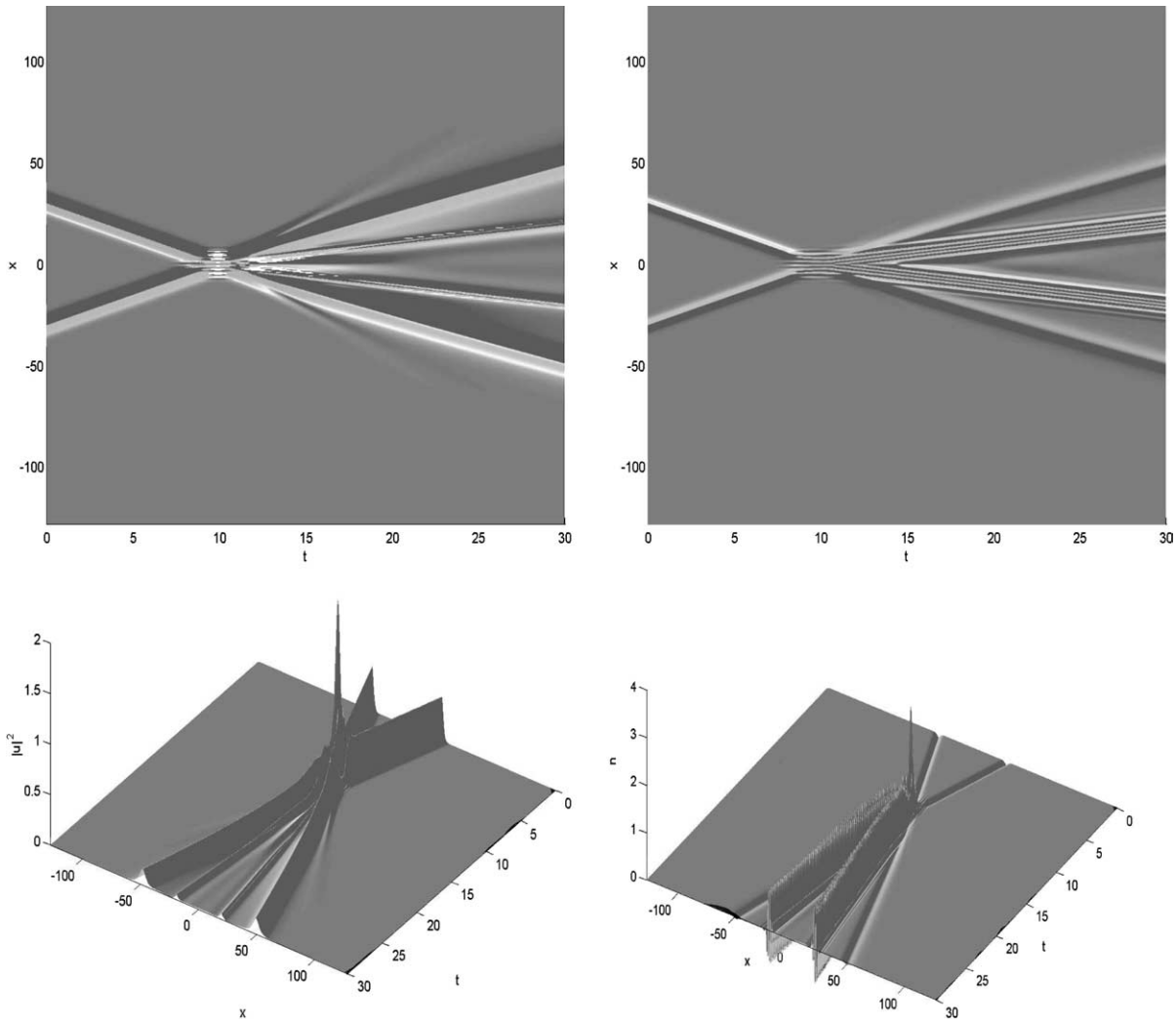

Fig. 10. $v = 3.0$, $\mu/\lambda = 1.45$. Left: $|u|^2$. Right: n.

First, we consider the collisions of two solitons with subsonic propagation speeds. As is known, when μ/λ is small, the generalized ZS is close to the cubically nonlinear Schrödinger equation (focusing for $\lambda > 0$). This implies that collision between solitons are quite elastic. After collision, two solitons form again and propagate in their original directions but with slightly smaller speeds (see Fig. 5). At the same time, from the n-plot, one can see that besides the dispersive wave propagating with the same speed as u, the collision also results in a pair of nondispersive waves, which travel with larger energy. With the growth of μ/λ, the new-formed solitons' speed becomes smaller (see Fig. 6), and a series of nondispersive waves are emitted from the collision point successively, traveling with much smaller energy. When μ/λ becomes even larger, after a critical value, the collision results in total fusion. Solitons are not generated again after collision. In addition, the fusion is accompanied with a series of strong emission of nondispersive waves (see Figs. 7 and

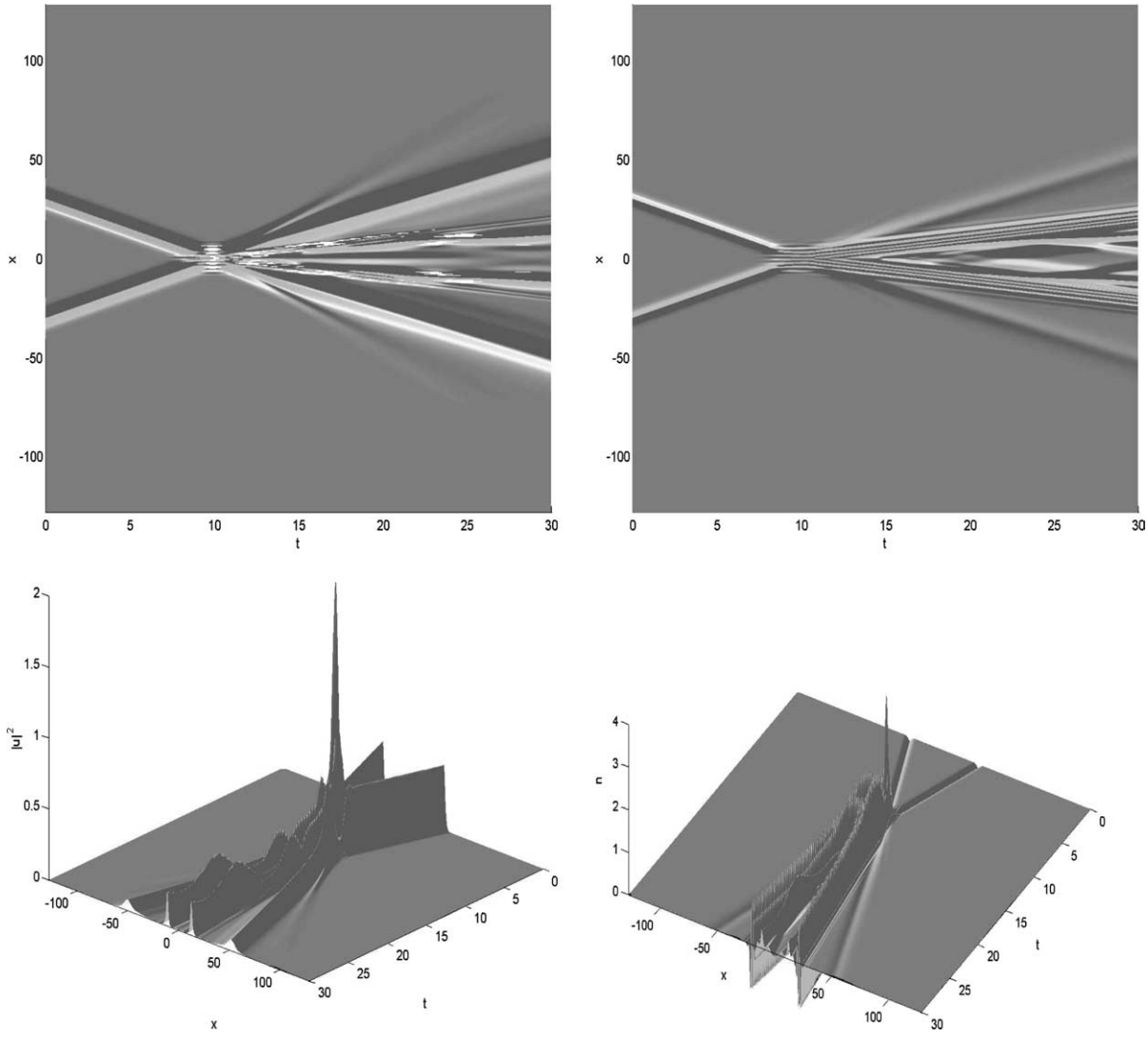

Fig. 11. $v = 3.0$, $\mu/\lambda = 1.75$. Left: $|u|^2$. Right: n.

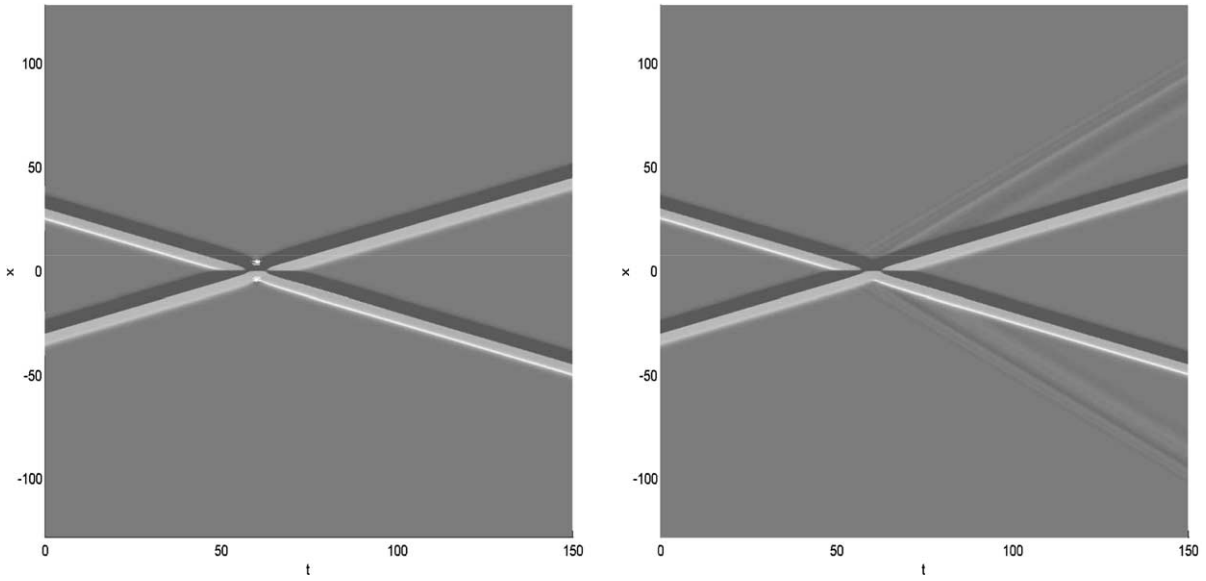

Fig. 12. $v = 0.5$, $\mu/\lambda = -0.8$. Left: $|u|^2$. Right: n.

8). Our computation shows that the critical value strongly depends on the soliton speed. We list part of the numerical results in Table 10. Notice that our numerical values for the critical value are somewhat different from those given in the paper [14], the later computed by finite difference schemes which are inferior to the spectral method as studied in [4].

These phenomena in the transsonic case are somewhat different. When μ/λ is small, the collision seems to be elastic and the departing speeds of the solitons formed after collision are almost the same as before collision (see Fig. 9). When μ/λ becomes larger, a pair of solitons with slower speed shows up (see Fig. 10). We call them slow solitons. In contrast, we call the solitons with a larger speed fast solitons. With further growth of μ/λ, the amplitude of slow solitons is increasing while the amplitude of fast solitons is decreasing. After a focal point, the amplitudes of slow solitons become larger than the fast ones (see Fig. 11). Besides, the speeds of slow solitons turn out to be smaller with the growth of μ/λ. In all the transsonic region, the radiative losses tend to be more severe with the growth of μ/λ.

- $\lambda < 0$, $\mu > 0$. In this case, only the subsonic soliton exists in the gap $c\sqrt{1 - \mu/|\lambda|} < |v| < c$, provided $\mu/|\lambda| < 1$. We consider the collisions of two solitons with equal initial phases. Our numerical experiments show that this case is much simpler than that we discussed above. All the collisions seem to be rather elastic and no significant radiation is observed. See Fig. 12.

References

[1] W. Bao, S. Jin, P.A. Markowich, On time-splitting spectral approximations for the Schrödinger equation in the semiclassical regime, J. Comput. Phys. 175 (2002) 487–524.
[2] W. Bao, S. Jin, P.A. Markowich, Numerical study of time-splitting spectral discretizations of nonlinear Schrödinger equations in the semi-classical regimes, SIAM J. Sci. Comput. 25 (2003) 27–64 (electronic).
[3] W. Bao, F.F. Sun, Numerical simulation of the vector Zakharov system for multi-component plasma, SIAM J. Sci. Comput. (to appear).
[4] W. Bao, F.F. Sun, G.W. Wei, Numerical methods for the generalized Zakharov system, J. Comput. Phys. 190 (2003) 201–228.
[5] R. Caflisch, S. Jin, G. Russo, Uniformly accurate schemes for hyperbolic systems with relaxations, SIAM J. Numer. Anal. 34 (1997) 246–281.

[6] C. Canuto, M.Y. Hussaini, A. Quarteroni, T.A. Zang, Spectral Methods in Fluid Dynamics, Springer, New York, 1988.
[7] H.D. Ceniceros, F.R. Tian, A numerical study of the semi-classical limit of the focusing nonlinear Schrödinger equation, Phys. Lett. A 306 (2002) 25–34.
[8] Q. Chang, H. Jiang, A conservative difference scheme for the Zakharov equations, J. Comput. Phys. 113 (1994) 309.
[9] Q. Chang, B. Guo, H. Jiang, Finite difference method for generalized Zakharov equations, Math. Comput. 64 (1995) 537.
[10] C.W. Gear, Numerical Initial Value Problems in Ordinary Differential Equations, Prentice-Hall, Englewood Cliffs, NJ, 1971.
[11] R. Glassey, Approximate solutions to the Zakharov equations via finite differences, J. Comput. Phys. 100 (1992) 377.
[12] R. Glassey, Convergence of an energy-preserving scheme for the Zakharov equations in one space dimension, Math. Comput. 58 (1992) 83.
[13] H. Hadouaj, B.A. Malomed, G.A. Maugin, Dynamics of a soliton in a generalized Zakharov system with dissipation, Phys. Rev. A 44 (6) (1991) 3925–3931.
[14] H. Hadouaj, B.A. Malomed, G.A. Maugin, Soliton–soliton collisions in a generalized Zakharov system, Phys. Rev. A 44 (6) (1991) 3932–3940.
[15] S. Jin, Runge–Kutta methods for hyperbolic conservation laws with stiff relaxation terms, J. Comput. Phys. 122 (1995) 51–67.
[16] D. Pathria, J.L. Morris, Pseudo-spectral solution of nonlinear Schrödinger equation, J. Comput. Phys. 87 (1980) 108–125.
[17] T. Ozawa, Y. Tsutsumi, The nonlinear Schrödinger limit and the initial layer of the Zakharov equations, Diff. Int. Eqn. 5 (1992) 721–745.
[18] G.L. Payne, D.R. Nicholson, R.M. Downie, Numerical solution of the Zakharov system, J. Comput. Phys. 50 (1983) 482–498.
[19] S. Schochet, M. Weinstein, The nonlinear Schrödinger limit of the Zakharov equations governing Langmuir turbulence, Commun. Math. Phys. 106 (1986) 569–580.
[20] G. Strang, On the construction and comparison of difference schemes, SIAM J. Numer. Anal. 5 (3) (1968) 506–517.
[21] C. Sulem, P.L. Sulem, The Nonlinear Schrödinger Equation, Springer, New York, 1999.